International Conference on Applied Energy 2021
Nov. 29 - Dec. 5, 2021, Thailand/Virtual
Paper ID: 585

Numerical Investigation of Copper Foam Adsorption Beds Packed With MOF-801 for Space Cooling and Desalination Applications

Mohamed Rezk [1], Mahmoud B. Elsheniti [1, 2], Ahmed Rezk [1, 3, 4] and Osama A. Elsamni [1]

1 Mechanical Engineering Department, Faculty of Engineering, Alexandria University, El-Chatby, Alexandria 21455, Egypt

2 Mechanical Engineering Department, College of Engineering, King Saud University, Riyadh 11451, KSA.

3 Energy and Bioproducts Research Institute (EBRI), College of Eng. and Physical Science, Aston University, Birmingham, B4 7ET, UK.

4 Aston Institute of Material Research (AIMR), College of Engineering and Physical Science, Aston University, Birmingham, B4 7ET, UK

ABSTRACT

In this paper, an emerging Metal Organic Framework adsorbent MOF-801 packed into a recently developed copper foamed adsorbent-bed is numerically investigated under different operating conditions and physical parameters and benchmarked against the widely used silica gel adsorbent. A numerical model using lumped dynamic modelling approach was developed and validated against experimental data. The results demonstrated an improvement in the overall performance of both MOF-801 and silica gel foam packed beds due to the enhancement in the effective thermal conductivity. The MOF-801-based system showed a higher performance for desalination applications with a maximum specific daily water production of 13 m^3/ton·day compared to 9.2 m^3/ton·day for the silica gel-based system. MOF-801-based system evidenced its competition in the cooling applications, achieving enhancement for the specific cooling power with average 40% higher than the silica gel-based system.

Keywords: adsorption cooling, desalination, MOF-801, silica gel, copper foam.

NONMENCLATURE

Abbreviations	
CC	Cooling Capacity (kW)
COP	The coefficient of performance
C_p	Specific heat capacity (J/kg k)
D_{so}	Surface diffusivity pre-exponent constant (m^2/s)
E_a	Activation energy of surface diffusion (J/kg)
HTF	Heat transfer fluid
K	Thermal conductivity (W/m K)
$K_s a_v$	Overall mass transfer coefficient (s^{-1})
K_o	Pre-exponential constant in (Pa^{-1})
M	Mass (kg)
R_p	Adsorbent particle radius (m)
$\overline{R}$	Universal gas constant (J/kg K)
SCP_{mass}	Specific cooling power per unit mass (W/kg_{ads})
SCP_{vol}	Specific cooling power per unit volume (kW/m^3)
SDWP	Specific daily water production (m^3/(ton.day))
Sg	Silica gel
T	Temperature (K)
t	Time (s)
W	Specific adsorption (kg/kg_{ads})
W_{eq}	Equilibrium adsorption uptake (kg/kg_{ads})
Subscripts	
ads	Adsorption
cond	Condenser
des	Desorption
evap	Evaporator
Hex	Heat exchanger
Ref	Refrigerant

1. INTRODUCTION

Nowadays, energy and freshwater resources face rising demands and constraints in many regions of the world due to the economic and population growth. It is predicted that around 52% of the world's population will face acute water scarcity by 2050 [1]. Freshwater scarcity leads to a greater reliance on alternative energy-intensive desalination systems (e.g., thermal, membrane and chemical desalination) to utilize brackish and seawater [2]. Besides, the current energy demand for

Selection and peer-review under responsibility of the scientific committee of the 13th Int. Conf. on Applied Energy (ICAE2021).

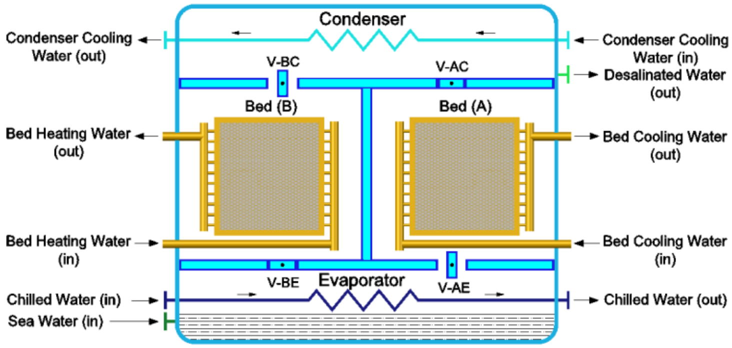

Fig. 1. Schematic diagram for the simulated adsorption chiller

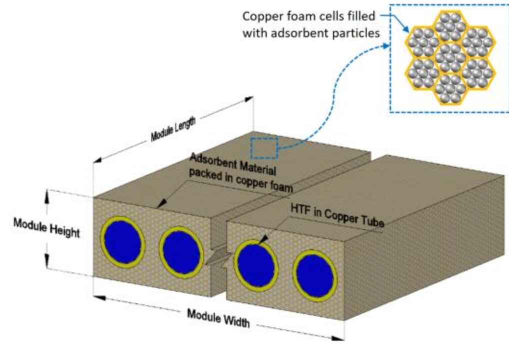

Fig. 2. Copper foam bed packed with adsorbent material with detailed copper foam cells filled with adsorbent particles

space cooling tripled since 1990 [3]. Of the global energy consumption, the prospected share of space cooling share is almost 16% by 2050 [4]. Additionally, the widely spread conventional cooling systems utilize long-lasting ozone-depleting and global warming refrigerants [5].

Adsorption cooling and desalination systems are the most feasible alternatives utilizing low-grade heat sources (50 - 90 ^{o}C), such as solar and waste energy [6]. In addition, adsorption cooling systems utilize eco-friendly working fluids, such as water, methanol and ethanol [7]. Nevertheless, such systems have the technical challenge of poor heat and mass transfer performance at the core component (i.e., adsorption bed) level, which leads to a relatively heavy and large physical footprint at the system level [8]. Also, the low COP, low SCP, and high initial cost hindered these systems from commercializing [9].

Many studies have been conducted to overcome these technical problems. Using metallic foams significantly improves the thermal conductivity for the adsorption bed. Pinheiroa et al. [10] investigated the using of copper foam coated with CPO-27(Ni) compared to AQSOATM FAM-Z02. The obtained COP and SCP_{mass} for the CPO-27(Ni)/copper foam were in range of 1.16-1.39 and 1922-5130 W/kg_{ads} which outperformed those of AQSOATM FAM-Z02/copper foam at the same operation conditions. Freni et al. [11] proposed a new adsorption bed configuration that consists of highly porous copper foams directly sintered on the external surface of copper pipes and coated with several layers of zeolite 4A. The results of the simulations provided a COP of 0.10-0.28, SCP_{mass} of 77-123 W/kg_{ads}, and SCP_{vol} of 103-214 kW/m^3. Mohammed et al. [12] investigated experimentally and numerically the adsorption and desorption process of silica gel with different particles sizes packed into aluminium foam bed with various pores per inch (PPI) under typical operating conditions. Advanced system performance was reported; SCP_{mass} of 827 W/kg_{ads}, a SCP_{vol} of 517 W/m^3, and a COP of 0.75 using 20 PPI aluminium foam.

Furukawa et al. [13] investigated a group of zirconium MOFs materials and evaluated their performers based on three criteria: water condensation at low relative pressure, high water uptake capacity, and high recyclability and water stability. Among these materials was MOF-801, which showed an excellent performance with an uptake capacity of 22.5 wt % at P/P_0 = 0.1. Solovyeva et al. [14] investigated MOF-801 for cooling application revealing a COP of 0.67 and a SCP_{mass} of 2000 W/kg_{ads}. Kim et al. [15] proposed a water harvest unit with activated MOF-801 in a porous copper foam that improved the overall bed thermal conductivity and enhanced the structural rigidity.

The emphasis of this work is to compare MOF-801, as an emerging adsorption material, and silica gel, each packed into a copper foamed bed (i.e., MOF-801/copper foam and silica-gel/copper foam), in a new conceptual bed design for adsorption cooling and desalination applications. A numerical model using the Matlab platform was used to study the influence of the proposed bed materials on the overall system performance under typical operating conditions for cooling and desalination applications. The influence of the operational and geometrical parameters was investigated by changing the operation cycle times at different bed heights.

2. SYSTEM DESCRIPTION

Fig. 1 shows a schematic diagram for the simulated two-bed adsorption system. Typically, each adsorbent bed is connected to the evaporator or condenser by flap valves operated by the pressure difference between heat exchangers during adsorption/evaporation and desorption/condensation. Fig. 2 illustrates the simulated adsorbent bed heat exchanger, consisting of plain copper tubes covered by rectangular copper foam packed with the adsorbent granules.

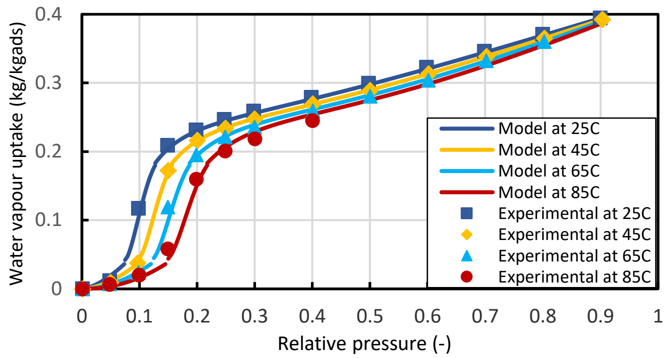

Fig. 3. Validation of proposed isotherm equations with the experimental data

2.1 *Adsorption isotherm*

The measured adsorption isotherms at temperatures (15 °C, 25 °C 45 °C and 65 °C) [15] were fitted using series of exponential and polynomial characteristic equations (1)-(3).

$$w^* = 2.18865 * \exp(-6.61855669E-4A) \qquad (A > 6200) \qquad (1)$$

$$w^* = 7.6163E-11A^3 - 1.240E-6A^2 + 6.5914E-3A - 11.297 \qquad (6200 \geq A \geq 4900) \qquad (2)$$

$$w^* = -1.763E-16A^4 - 1.2384E-12A^3 + 2.2088E-8A^2 - 1.0597E-4A + 0.419 \qquad (A < 4900) \qquad (3)$$

Where w* is the uptake value at equilibrium conditions, and A is the adsorption potential, Eq (4).

$$A = \bar{R}T\ln(P/P_s)(0.002 \times (T-318)) + 1) \qquad (4)$$

(P/P_s) denotes the evaporator/bed or condenser/bed pressure ratio during the adsorption and desorption process. The term (0.002*(T-318)+1) is a correlation factor for fitting the measured isotherms with the proposed equations. Fig. 3 shows the validation for the predicted characteristic equations for MOF-801.

2.2 *Adsorption Kinetics*

The linear driving force model (LDF) Eqs. (5)-(7), as per Sakoda and Suzuki [16] were used to predict the rate of adsorption/desorption (dw/dt) using the temporal experimentally measured water fractional uptake curves [15].

$$dw/dt = k_s a_v (w^* - w) \qquad (5)$$

$$k_s a_v = k_0 \exp(-E_a/\bar{R}T) \qquad (6)$$

$$k_0 = F.D_{so}/R_p^2 \qquad (7)$$

The calculated kinetic parameters for MOF-801 in this work and the parameters for silica gel used by Rezk et al. [17] are furnished in Table 1. Fig. 4 shows the validation for the predicted kinetic curves parameters with the measured curves for MOF-801.

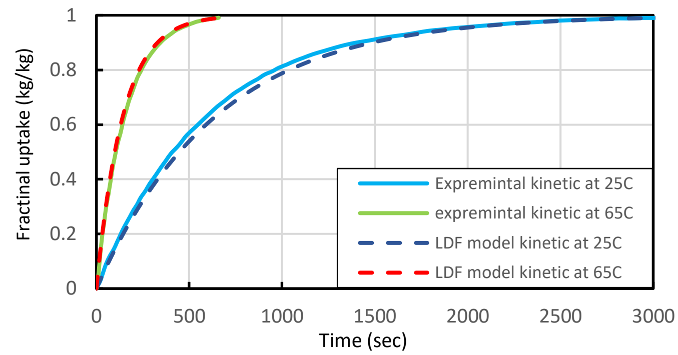

Fig. 4. Validation of proposed LDF kinetic parameters with the measured uptake curves at partial pressure 25%

Table 1 Linear driving force, LDF equation constants.

Symbol	MOF-801 (This work)	Silica gel [17]	Unit
$F.D_{so}$	$1.30558\text{x}10^{-10}$	3.81x10-3	m/s^2
E_a	$3.1533\text{x}10^4$	$4.2\text{x}10^4$	J/mol
R_p	$5\text{x}10^{-7}$	$0.16\text{x}10^{-3}$	m
k_0	522.23	$2.939\text{x}10^6$	s^{-1}

2.3 *Adsorption chiller modelling.*

It was assumed that: the adsorbent, adsorbate and heat exchanger metal are instantaneously at the same temperature, neglecting the heat and mass transfer to the surroundings. The energy balance equations for adsorption/desorption beds, evaporator and condenser are illustrated in Eqs. (8)-(10) [18]. Fig. 5 shows the flow chart for the system modelling.

$$\left(\xi M_{w,ads} Cp_w(T_{bed}) + M_{ads} w_{bed} Cp_{ref}(T_{bed}) + M_{ads} Cp_{ads} + M_{Hex,bed} Cp_{Hex,bed}\right)\frac{dT_{bed}}{dt} = (\phi.\partial)M_{ads}\frac{dw_{bed}}{dt}\left[\gamma\{h_g(T_{Hex}) - h_g(P_{Hex},T_{bed})\} + (1-\gamma)\{h_g(P_{Hex},T_{bed}) - h_g(P_{bed},T_{bed})\}\right] + \phi M_{ads}\frac{dw_{bed}}{dt}\Delta H_{ads} + (1-\xi)\sum_{n=1}^{n=N_{bed}} dUA_{bed,k} \times LMTD_{bed} \qquad (8)$$

$$\left(Cp_{ref,f}(T_{evap})M_{ref,evap} + M_{Hex,evap}Cp_{Hex,evap}\right)\frac{dT_{evap}}{dt} = UA_{evap} \times LMTD_{evap} + \frac{d}{dt}E_{pump}\phi M_{ads}\frac{dw_{bed}}{dt}\left[\left(h_{ref,evap,in} - h_{ref,evap,out}\right)\right] \qquad (9)$$

$$\left(Cp_{ref,l}(T_{cond})M_{ref,cond} + M_{Hex,cond}Cp_{Hex,cond}\right)\frac{dT_{cond}}{dt} = UA_{cond} \times LMTD_{cond} + \phi M_{ads}\frac{dw_{bed}}{dt}\left[\left(h_{ref,cond,l} - h_{ref,cond,g}\right) + Cp_{ads}(T_{cond} - T_{bed})\right] \qquad (10)$$

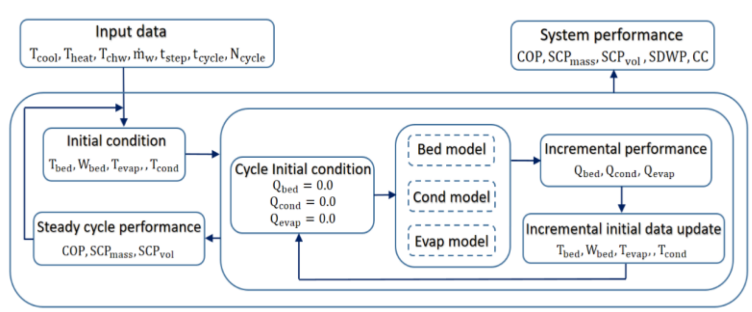

Fig. 5. System modelling flow chart

2.4 Bed thermal resistance

Fig. 6 (A) shows a control volume of an incremental element from the adsorber bed. Each element consists of a copper tube surrounded by adsorbent material/copper foam. Fig. 6 (B) presents a schematic diagram for the bed heat transfer resistances during the heat transfer from/to the heat transfer fluid (HTF) to/from the surrounded vapor during desorption/adsorption modes. There are five heat transfer resistances: (R1) radial convection thermal resistance from the HTF fluid stream to the internal tube wall, (R2) radial conduction thermal resistance through the tube wall, (R3) contact thermal resistance between the adsorbent material and tube outside surface and (R4 and R5) two conduction thermal resistances through the adsorbent material in the radial and the axial directions, respectively. The incremental axial conduction thermal resistance through the tube wall was neglected due to its insignificant effect compared to other resistances.

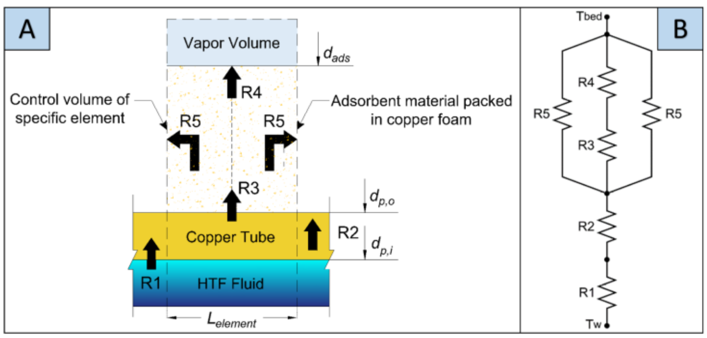

Fig. 6. (A) Control volume of an element in the adsorber bed, (B) Heat transfer resistance schematic diagram.

The mathematical formulas of the heat transfer resistances are illustrated in Eqs: (11)-(15).

$$R_1 = 1/\left(htc_{i,bed}A_{i,bed}\right) \quad (11)$$

$$R_2 = \left[\ln(d_{p,o} - d_{p,i})\right]/(2\pi k_t L_{element}) \quad (12)$$

$$R_3 = R_{cont}/(\pi d_o L_{element}) \quad (13)$$

$$R_4 = \left[\ln(d_{ads}/d_{p,o})\right]/(2\pi k_{ads} L_{element}) \quad (14)$$

$$R_5 = (L_{element}/2)/(A_{ads} k_{ads}) \quad (15)$$

Where htc, A, d, k, R_{cont} and $L_{element}$ denote the convection heat transfer coefficient, surface area, diameter, thermal conductivity, contact thermal resistance and adsorbent element thickness, respectively. Subscripts i, o, t, and ads refer to inside, outside, tube, and adsorbent.

3. RESULTS

The influence of changing the operational and geometrical parameters on the overall performance for the adsorption cooling and desalination systems with using MOF-801/copper foam comparing to silica-gel/copper foam as adsorption materials were investigated. The effect of the cycle time on the operation performance was studded from 200 s to 1000 s at different bed heights from 20 mm to 32 mm. Fig. 7 to Fig. 10 show the impact of the cycle time and bed height on the SDWP, CC, SCP_{mass} and SCP_{vol} for both materials. The heating, cooling, and chilled water temperatures were kept constant at 85 °C, 30 °C, and 15 °C, respectively.

3.1 The water and cooling production (SDWP and CC)

Fig. 7 shows that the SDWP for the MOF-801 outperforming silica gel at all cycle times and bed heights. The maximum SDWP for both materials occurs at bed height 20 mm to be 13 m^3/(ton.day) for MOF-801 at cycle time 300 s compared to 9.2 m^3/(ton.day) for silica gel at cycle time 200 s. The outperforming performance of the MOF-801 for water production stemmed from its steep isotherm curve, which increases its cycling adsorption uptake compared to silica gel at the same cycle times, as shown in Fig. 11. Referring to the difference of the packing densities between the two materials, the mass of the silica gel exceeds MOF-801 for the same bed size. For example, the mass of MOF-801 equals 31.2 kg compared to 46.5 kg for silica gel at bed height 20 mm. Despite this mass difference, the CC for MOF-801 exceeded silica gel at most operation conditions, as shown in Fig. 8. It is noted that the gap of CC between MOF-801 and silica gel is decreasing with the decrease of the cycle times and the decrease of the bed height which makes the CC for the silica gel exceeds that of MOF-801 at cycle times below 400 s for bed heights from 20 mm to 24 mm. The maximum CC for both materials was achieved at bed height 32 mm to be 16 kW at cycle time 400 s for MOF-801 and 15.2 kW at cycle time 300 s for silica gel.

3.2 The specific cooling powers per unit mass and per unit volume (SCP_{mass} and SCP_{vol})

Fig. 9 shows that SCP_{mass} for MOF-801 outperforming silica gel at all cycle times and bed heights owing to the high cyclic uptake capacity for MOF-801 compared to silica gel. The maximum SCP_{mass} achieved was at bed height 20 mm to be 365 W/kg for MOF-801 at cycle time 300 s compared to 267 W/kg for silica gel at cycle time 200 s. As shown in Fig. 10, the SCP_{vol} for MOF-801 exceeded that of silica gel at cycle times more than 400 s for all bed heights. Notably, the increase of the SCP_{vol} for silica gel is more rapidly with the decreasing cycle times

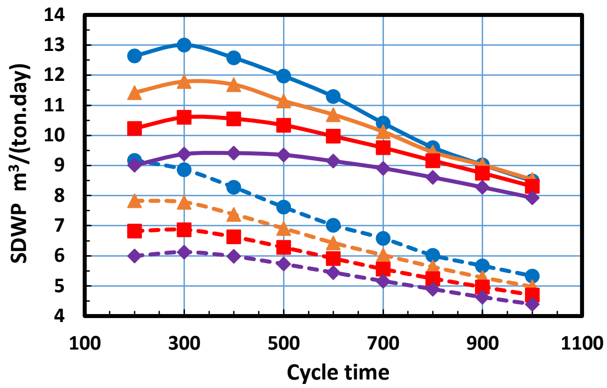

Fig. 7. MOF-801 and Silica-gel each with copper foam (SDWP)

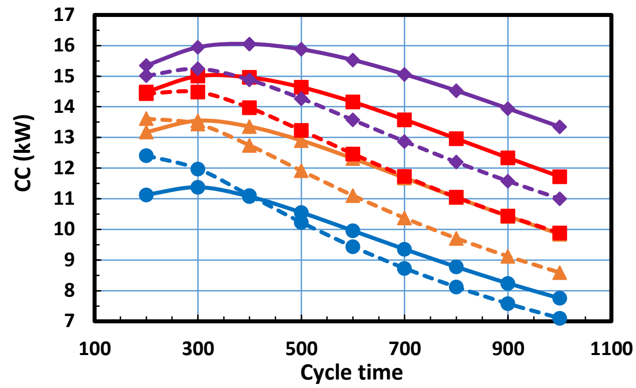

Fig. 8. MOF-801 and Silica-gel each with copper foam (CC)

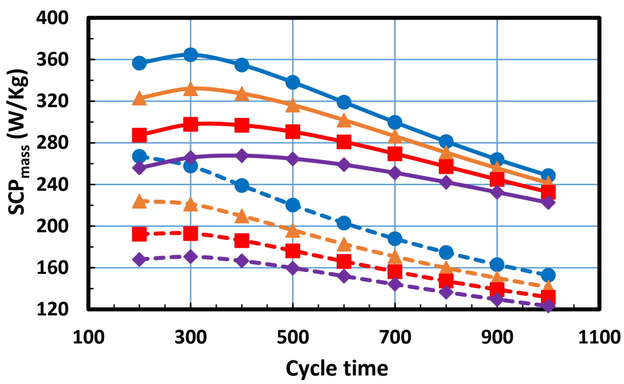

Fig. 9. MOF-801 and Silica-gel each with copper foam (SCP_{mass})

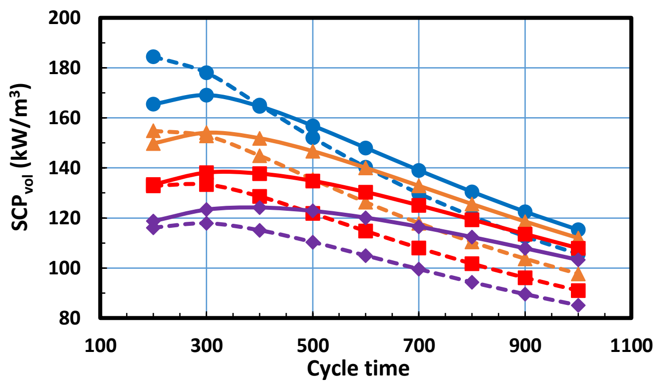

Fig. 10. MOF-801 and Silica-gel each with copper foam (SCP_{vol})

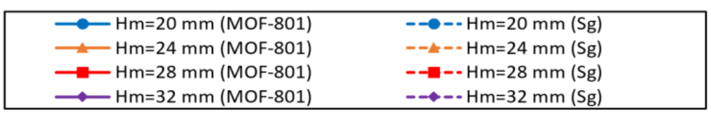

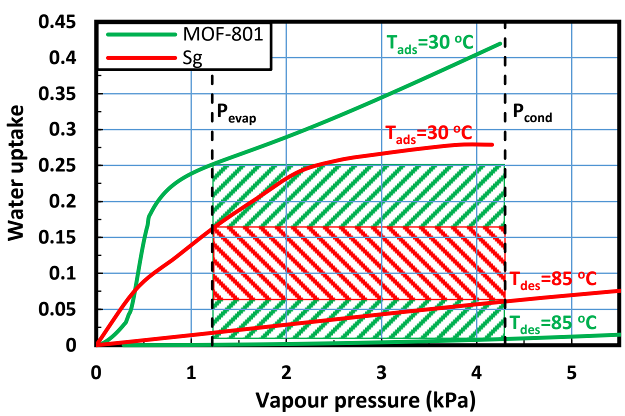

Fig. 11. Isotherms comparison with ideal cycle superimposed

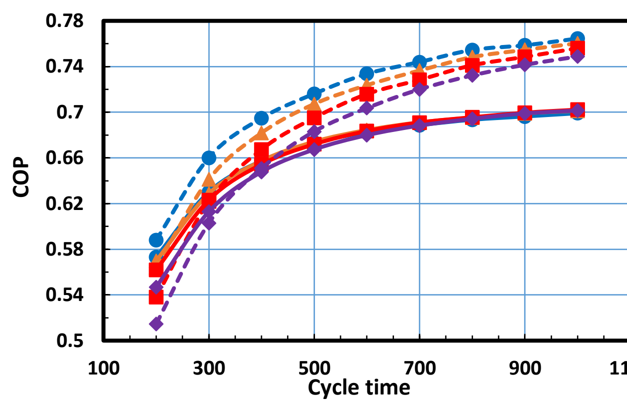

Fig. 12. MOF-801 and Silica-gel each with copper foam (COP)

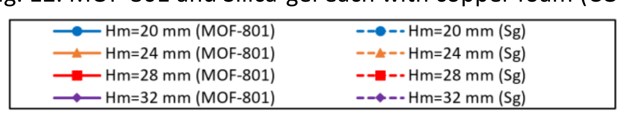

compared to MOF-801, which makes the SCP_{vol} for the silica gel exceed MOF-801 at cycle time 200 s and bed heights less than 28 mm. The maximum SCP_{vol} occurs for both materials at bed height 20 mm, reaching 185 kW/m^3 for silica gel at cycle time 200 s and 169 kW/m^3 for MOF-801 at cycle time 300 s.

3.3 The Coefficient of performance (COP)

Decreasing the bed heights showed a more significant influence on the COP of silica gel compared to that of MOF-801. The COP of silica gel outperformed that of MOF-801 for cycle times more than 400 s at all bed heights, as shown in Fig. 12. For low cycle times as in 200 s, the COP of MOF-801 exceeds that of silica gel for bed height more than 24 mm. The maximum COP for silica gel and MOF-801 is 0.76, 0.7 respectively occurred for both materials at cycle time 1000 s and bed height 20 mm.

4. *CONCLUSION*

This study compared MOF-801 and silica gel packed into a newly developed copper foamed bed for adsorption cooling and desalination applications while changing the cycle times and the bed heights. The following conclusions were drawn:

1. The contribution of the copper foams significantly influenced the bed thermal conductivity and improved the overall operation performance for both materials.
2. MOF-801 outperformed silica gel in water desalination applications, achieving a maximum SDWP of 13 $m^3/(ton \cdot day)$ compared to 9.2 $m^3/(ton \cdot day)$ for the silica gel.
3. MOF-801 evidences its capability for cooling applications compared to silica gel with maximum SCP_{mass} and SCP_{vol} of 365 W/kg and 169 kW/m^3 compared to 267 W/kg and 185 kW/m^3 for silica gel, respectively.
4. Silica gel achieved a higher COP than MOF-801 at the cycle times more than 400 s for all studied bed heights with a maximum COP of 0.76 for silica gel compared to 0.7 for MOF-801 at cycle time 1000 s.

REFERENCE

[1] UN World Water Development Report 2020: Water and Climate Change. (UNESCO); Available from: https://www.unwater.org/publications/world-water-development-report-2020/.
[2] Introduction to the water-energy nexus, Paris 2020, (International Energy Agency); Available from: https://www.iea.org/articles/introduction-to-the-water-energy-nexus.
[3] Cooling, Paris 2020, (International Energy Agency); Available from: https://www.iea.org/reports/cooling.
[4] The Future of Cooling, Paris 2018, (International Energy Agency); Available from: https://www.iea.org/reports/the-future-of-cooling.
[5] Elsheniti MB, Abd El-Hamid AT, El- Samni OA, Elsherbiny SM, Elsayed E, Experimental evaluation of a solar two-bed lab-scale adsorption cooling system. 2021; 60(3):2747-2757. (Alexandria Engineering Journal)
[6] Elsheniti MB, Rezk A, Shaaban M, Roshdy M, Nagib YM, Elsamni OA, Saha BB, Performance of a solar adsorption cooling and desalination system using aluminum fumarate and silica gel. 2021; 194:117116. (Applied Thermal Engineering)
[7] Chekirou W, Chikouche A, Nahman B, Ahcène K, Phalippou S, Dynamic modelling and simulation of the tubular adsorber of a solid adsorption machine powered by solar energy. 2014; 39:137-151. (Int J Refrig)
[8] Smith DS, Alzina A, Bourret J, Nait-Ali B, Pennec F, Tessier-Doyen N, Otsu K, Matsubara H, Elser P, Gonzenbach UT, Thermal conductivity of porous materials. 2013; 28(17):2260-2272. (Journal of Materials Research)
[9] ul Qadir N, Said SAM, Mansour RB, Modeling the performance of a two-bed solar adsorption chiller using a multi-walled carbon nanotube/MIL-100(Fe) composite adsorbent. 2017; 109:602-612. (Renewable Energy)
[10] Pinheiro JM, Salústio S, Geraldes V, Valente AA, Silva CM, Copper foam coated with CPO-27(Ni) metal–organic framework for adsorption heat pump: Simulation study using OpenFOAM. 2020; 178:115498. (Applied Thermal Engineering)
[11] Freni A, Bonaccorsi L, Proverbio E, Maggio G, Restuccia G, Zeolite synthesised on copper foam for adsorption chillers: A mathematical model. 2009; 120(3):402-409. (Microporous and Mesoporous Materials)
[12] Mohammed RH, Mesalhy O, Elsayed ML, Chow LC, Performance enhancement of adsorption beds with silica-gel particles packed in aluminum foams. 2019; 104:201-212. (International Journal of Refrigeration)
[13] Furukawa H, Gándara F, Zhang Y-B, Jiang J, Queen WL, Hudson MR, Yaghi OM, Water Adsorption in Porous Metal–Organic Frameworks and Related Materials. 2014; 136(11):4369-4381. (Journal of the American Chemical Society)
[14] Solovyeva MV, Gordeeva LG, Krieger TA, Aristov YI, MOF-801 as a promising material for adsorption cooling: Equilibrium and dynamics of water adsorption. 2018; 174:356-363. (Energy Conversion and Management)
[15] Kim H, Rao SR, Kapustin EA, Zhao L, Yang S, Yaghi OM, Wang EN, Adsorption-based atmospheric water harvesting device for arid climates. 2018; 9(1). (Nature Communications)
[16] Sakoda A, Suzuki M, FUNDAMENTAL STUDY ON SOLAR POWERED ADSORPTION COOLING SYSTEM. 1984; 17(1):52-57. (Journal of Chemical Engineering of Japan)
[17] Rezk A, Al-Dadah R, Mahmoud S, Elsayed A, Characterisation of metal organic frameworks for adsorption cooling. 2012; 55(25):7366-7374. (International Journal of Heat and Mass Transfer)
[18] Rezk A, Al-Dadah RK, Mahmoud S, Elsayed A, Effects of contact resistance and metal additives in finned-tube adsorbent beds on the performance of silica gel/water adsorption chiller. 2013; 53(2):278-284. (Applied Thermal Engineering)